Heliyon 10 (2024) e35362

Contents lists available at ScienceDirect

Heliyon

journal homepage: www.cell.com/heliyon

Research article

Absence of PNET formation and normal longevity in a mouse model of Mahvash disease

Yingna Xu [a], Qiaofeng Liu [b], Chuan-Wei Chen [c], Qiuying Wang [d], Tianyuan Du [d], Run Yu [e], Qingtong Zhou [a,c], Dehua Yang [c,d,f,**], Ming-Wei Wang [a,c,g,h,*]

[a] Department of Pharmacology, School of Basic Medical Sciences, Fudan University, Shanghai, 200032, China
[b] School of Pharmacy, Fudan University, Shanghai, 201203, China
[c] Research Center for Deepsea Bioresources, Sanya, Hainan, 572025, China
[d] School of Chinese Materia Medica, Nanjing University of Chinese Medicine, Nanjing, 210023, China
[e] Division of Endocrinology, Diabetes, and Metabolism, David Geffen School of Medicine at UCLA, Los Angeles, CA, 90095, USA
[f] State Key Laboratory of Chemical Biology, Shanghai Institute of Materia Medica, Chinese Academy of Sciences, Shanghai, 201203, China
[g] Department of Chemistry, School of Science, The University of Tokyo, Tokyo, 113-0033, Japan
[h] Engineering Research Center of Tropical Medicine Innovation and Transformation of Ministry of Education, School of Pharmacy, Hainan Medical University, Haikou, 570228, China

ARTICLE INFO

Keywords:
Glucagon
Glucagon receptor
Amino acid
Metabolism
Mahvash disease

ABSTRACT

Mahvash disease, a rare autosomal recessive metabolic disorder characterized by biallelic loss-of-function mutations in the glucagon receptor gene (*GCGR*), induces significant pancreatic hyperglucagonemia, resulting in α-cell hyperplasia and occasional hypoglycemia. Utilizing CRISPR-Cas9 technology, we engineered a mouse model, designated as $Gcgr^{V369M/V369M}$, harboring a homozygous V369M substitution in the glucagon receptor (GCGR). Although wild-type (WT) and $Gcgr^{V369M/V369M}$ mice exhibited no discernible difference in appearance or weight, adult $Gcgr^{V369M/V369M}$ mice, approximately 12 months of age, displayed a notable decrease in fasting blood glucose levels and elevated the levels of cholesterol and low-density lipoprotein-cholesterol. Moreover, plasma amino acid levels such as alanine (Ala), proline (Pro) and arginine (Arg) were elevated in $Gcgr^{V369M/V369M}$ mice contributing to α-cell proliferation and hyperglucagonemia. Despite sustained α-cell hyperplasia and increased circulating glucagon levels in $Gcgr^{V369M/V369M}$ mice, metabolic disparities between the two groups gradually waned with age accompanied by a reduction in α-cell hyperplasia. Throughout the lifespan of the mice (up to approximately 30 months), pancreatic neuroendocrine tumors (PNETs) did not manifest. This prolonged observation of metabolic alterations in $Gcgr^{V369M/V369M}$ mice furnishes valuable insights for a deeper comprehension of mild Mahvash disease in humans.

1. Introduction

Glucagon (GCG), a polypeptide consisting of 29 amino acids and released by α-cells of the pancreatic islet, functions via activating

* Corresponding author. Research Center for Deepsea Bioresources, Sanya, Hainan, 572025, China.
** Corresponding author. State Key Laboratory of Chemical Biology, Shanghai Institute of Materia Medica, Chinese Academy of Sciences, Shanghai, 201203, China.
E-mail addresses: dhyang@simm.ac.cn (D. Yang), mwwang@simm.ac.cn (M.-W. Wang).

https://doi.org/10.1016/j.heliyon.2024.e35362
Received 23 June 2024; Accepted 26 July 2024
Available online 26 July 2024

the glucagon receptor (GCGR) mainly in the liver and kidneys [1]. It regulates processes such as glycogenolysis, gluconeogenesis and fatty acid oxidation by increasing intracellular cyclic adenosine monophosphate (cAMP) and calcium ion (Ca^{2+}) concentrations. Additionally, GCG plays a role in reducing triglyceride and cholesterol levels while balancing the release of low-density lipoprotein (LDL) [2]. Disruption of the GCGR gene (*GCGR*) or inhibition of GCGR signaling pathway can lead to α-cell hyperplasia, potentially progressing to pancreatic neuroendocrine tumors (PNETs) [3,4]. Previous research has elucidated a liver–α-cell axis, wherein GCGR antagonism decreases hepatic amino acid catabolism, raises circulating amino acid levels, and induces α-cell hyperplasia in a mammalian target of rapamycin (mTOR)-dependent manner [5].

Mahvash disease is associated with a homozygous inactivating GCGR mutation, causing pronounced hyperglucagonemia and α-cell hyperplasia often accompanied by intermittent hypoglycemia. While glucagonoma symptoms may not be evident initially, there is a potential for progression to glucagonoma and/or PNETs [6]. There exist nine naturally occurring mutations of GCGR [7]. Among these, the residue V368, located in transmembrane helix 6, indirectly influences the interaction between the N terminus of GCG and the extracellular loop 3 (ECL3) of GCGR by forming a hydrophobic pocket. The missense variant (V368M) disrupts this hydrophobic network, resulting in an increased distance between ECL3 and the N terminus of GCG [8]. Using CRISPR-Cas9 technology, we generated a mouse model of Mahvash disease by introducing a homozygous V369M substitution in the mouse GCGR (*Gcgr*$^{V369M/V369M}$), equivalent to the human GCGR mutation V368M. In previous studies, we observed reduced ligand binding and decreased GCG signaling in primary hepatocytes from *Gcgr*$^{V369M/V369M}$ mice [9]. These *Gcgr*$^{V369M/V369M}$ mice, regardless of being on a standard chow diet (SCD) or high-fat diet (HFD), displayed α-cell hyperplasia and elevated levels of glucagon (hyperglucagonemia) in the blood around 9 months of age [9,10]. Given the absence of established animal models for Mahvash disease, the potential progression to PNETs remains unknown. Therefore, we conducted this study to examine the long-term metabolic changes as well as morphology and histology of the pancreas and liver in *Gcgr*$^{V369M/V369M}$ mice under a regular chow diet (RCD) from 2- to 26-month of age, until their natural demise.

2. Materials and methods

2.1. Animals and diets

The generation of *Gcgr*$^{V369M/V369M}$ mice has been documented in a previous study (Figs. S1A–C) [9]. Verification of the genotypes for all the mice were confirmed through PCR and DNA sequencing (Fig. S1D). The mice were kept in a specific-pathogen–free (SPF) animal facility, adhering to a 12-h light/dark cycle at the vivarium within the Shanghai Institute of Materia Medica, Chinese Academy of Sciences. Male mice were utilized, with offspring from wild-type (WT) littermates serving as controls for the *Gcgr*$^{V369M/V369M}$ mice. Mice having *ad libitum* access to RCD and water.

2.2. Metabolic studies

Body weight and overnight fasting blood glucose levels were recorded monthly. Following an overnight fasting, blood was collected from the tail vein and subjected to blood glucose level measurement using the Accu-Chek blood glucose meter (Roche Diagnostics, Basel, Switzerland). Hemoglobin A1c (HbA1c) levels were assessed using the DCA Vantage analyzer (Vantage analyzer, Berlin, Germany). Oral glucose tolerance tests were conducted by administering glucose at a dosage of 2 g/kg body weight to male mice fasted for 6 h.

2.3. Histology

The pancreases and livers from the mice were harvested, preserved in 4 % paraformaldehyde (PFA), and embedded in paraffin. The samples were sliced into 4 μm thick sections. Each section of the pancreas and liver was stained with hematoxylin and eosin (H&E) following an established protocol [11]. The histological features of the liver and pancreas were evaluated and scored in accordance with the criteria described in a prior publication [10]. Pathological diagnoses were categorized into four levels: minor (+), mild (++), moderate (+++) and severe (++++) lesions.

2.4. Immunofluorescence

Before immunolabeling, the sections underwent sequential treatment with 3 % hydrogen peroxide, citrate antigen retrieval solution (Beyotime Biotechnology, Shanghai, China), and goat serum blocking solution successively. Insulin was stained using anti-insulin antibodies (1:200; Cell Signaling Technology, Danvers, MA, U.S.A.), while GCG was stained with anti-glucagon antibodies (1:200; Santa Cruz, Dallas, TX, U.S.A.). Subsequently, the sections were treated with Alexa Fluor 488-conjugated donkey anti-rabbit and Alexa Fluor 555-conjugated donkey anti-mouse IgG antibodies (Invitrogen, Waltham, MA, U.S.A.) at a 1:1000 dilution. Nuclei were then counterstained using 4′,6-diamidino-2-phenylindole (DAPI) (Invitrogen, Waltham, MA, U.S.A.). Analysis of the sections was performed using a Vectra automated quantitative pathology system (PerkinElmer, Waltham, MA, U.S.A.).

2.5. Blood chemistry

Starting from the second month, blood samples were collected monthly and stored at −80 °C. Plasma levels of albumin (ALB),

alanine aminotransferase (ALT), aspartate aminotransferase (AST), high-density lipoprotein-cholesterol (HDL-C), low-density lipoprotein-cholesterol (LDL-C), total cholesterol (TC) and triglycerides (TG) were measured using a JCA-BM6010/C analyzer (JEOL Ltd., Tokyo, Japan).

2.6. Hormone measurement

Whole blood from mice after overnight fasting was collected in EDTA-coated tubes. Plasma was separated by centrifugation at 12,000 rpm and stored at −80 °C until assayed. The levels of GCG, insulin and glucagon-like peptide-1 (GLP-1) were determined using a Mouse Glucagon ELISA Kit (Crystal Chem, Cook, IL, U.S.A.), Mouse Insulin ELISA Kit (Crystal Chem) and Mouse GLP-1 ELISA Kit (Crystal Chem), respectively.

2.7. Amino acid analysis

Amino acid levels were analyzed using the TRAQ™ reagent application Kit (AB Sciex, Framingham, MA, U.S.A.). Initially, 40 μL of plasma was mixed with 10 μL of sulfosalicylic acid and centrifuged at 10,000×*g* for 2 min. Following centrifugation, the supernatant was combined with 40 μL of labeling buffer and mixed by vortex. This mixture was then centrifuged again, and 10 μL of the diluted supernatant was mixed with 5 μL of diluted TRAQ™ reagent Δ8 and incubated at room temperature for 0.5 h. Subsequently, 5 μL of hydroxylamine was added. These samples were then dried completely in a centrifugal vacuum concentrator, which typically took less than 1 h. After drying, 32 μL of reconstituted amino acid internal standard solution was added to each TRAQ™ reagent Δ8-labeled sample. The final samples were centrifuged and analyzed using a 4000 QTRAP LC/MS/MS (Sciex, Redwood City, CA, U.S.A.).

2.8. RNA-sequencing (RNA-seq)

Pancreatic tissues were harvested from both WT and *Gcgr*$^{V369M/V369M}$ mice at 12 months of age. Total RNA was extracted from all samples using TRIzol® Reagent (Invitrogen, Waltham, MA, U.S.A.), following the manufacturer's instructions. RNA purification, reverse transcription, library construction, and sequencing were performed by Shanghai Majorbio Bio-pharm Biotechnology Co., Ltd. (Shanghai, China). For sequencing, the Illumina® Stranded mRNA Prep Ligation Kit (Illumina, San Diego, CA, U.S.A.) was employed for preparing the transcriptome library. The libraries were then amplified using a 15-cycle PCR and quantified with Qubit 4.0. Finally, the paired-end RNA-seq sequencing library was sequenced using the NovaSeq 6000 sequencer (Illumina, San Diego, CA, U.S.A.).

2.9. Bioinformatics analysis

The raw paired end reads were trimmed and quality controlled by the tool fastp [12]. The clean reads were then aligned to the reference genome in orientation mode by HISAT2 software [13]. Following alignment, the mapped reads of each sample were assembled using a reference-based approach with StringTie [14].

Gene abundances were quantified using RSEM [15]. Differentially expressed genes (DEGs) were identified using statistical significance assessed by DESeq2 [16] or DEGseq [17]. Genes with an absolute log2 fold change ($|\log2FC|$) of ≥ 1 and false discovery rate (FDR) of ≤ 0.05 (DESeq2) or FDR of ≤ 0.001 (DEGseq) were considered significantly differentially expressed (Table S4). Additionally, functional-enrichment analysis, including Gene Ontology (GO) and Kyoto Encyclopedia of Genes and Genomes (KEGG) pathway analyses, was conducted to identify significant enrichment of DEGs in GO terms and metabolic pathways. This analysis was performed at a Bonferroni-corrected P value of ≤ 0.05 compared to the whole-transcriptome background. GO functional enrichment analysis was conducted using Goatools, while KEGG pathway analysis was performed using KOBAS [18].

2.10. Real-time qRT-PCR

GADD45G mRNA expression levels were assessed via quantitative reverse transcription polymerase chain reaction (qRT-PCR). Total RNA was extracted from pancreatic tissue specimens, consistent with those utilized for RNA-seq, and subsequently converted into cDNA. The reverse transcription process followed established protocols to ensure reproducibility and accuracy. Real-time PCR was performed utilizing the LIFE VIIA7 Real-time PCR System (Applied Biosystems, Waltham, MA, U.S.A.) in conjunction with SYBR qPCR Master Mix (Vazyme, Nanjing, China) according to the manufacturer's instructions. Data analysis was carried out with QuantStudio Real-time PCR Software v1.3. *GADD45G* expression levels were normalized to β-actin and expressed as relative levels. The primers used are listed in Table S5.

2.11. Statistical analysis

Statistical analyses were conducted using GraphPad Prism 8 software (GraphPad, San Diego, CA, U.S.A.). The clustering of amino acid clustering was analyzed using MetaboAnalyst 5.0. The Kaplan–Meier method was used for the overall survival analysis. Statistical significance was assessed using a two-tailed Student's *t*-test, with a significance threshold of $P < 0.05$. The data presented are expressed as means ± standard error of the mean (S.E.M.) from multiple experiments conducted in duplicate.

3. Results

3.1. General characteristics of *Gcgr*$^{V369M/V369M}$ mice

Gcgr$^{V369M/V369M}$ mice did not display gross abnormalities compared with the WT (Fig. 1I). Unlike the lean phenotype observed in *Gcgr*$^{-/-}$ mice [6], *Gcgr*$^{V369M/V369M}$ mice exhibited increased body weight compared with the controls starting from 9 months of age, but this difference was not statistically significant after 11 months of age (Fig. 1A). Noticeable reductions in fasting blood glucose and HbA1c levels were observed in *Gcgr*$^{V369M/V369M}$ mice from 6 months of age onwards, persisting throughout the adulthood and diminishing with aging (Fig. 1B and C). Patient with Mahvash disease, harboring the homozygous c.958_960del (p. Phe320del) variant in GCGR, exhibit hypercholesterolemia, characterized by elevated LDL-C alongside normal triglyceride and HDL-C levels [19]. Similarly, *Gcgr*$^{V369M/V369M}$ mice showed a significant increase in total cholesterol and LDL-C levels around 11–20 months of age, with minimal changes in triglyceride and HDL-C levels (Fig. 1D–G). At the age of 12 months, *Gcgr*$^{V369M/V369M}$ mice demonstrated enhanced oral glucose tolerance compared to WT mice (Fig. 1H), indicating compromised GCGR function in regulating glucose homeostasis due to V369M mutation.

3.2. Pathological changes in the liver

At 3 months of age, *Gcgr*$^{V369M/V369M}$ mice exhibited liver steatosis and cytoplasmic glycogen content comparable to that of WT mice. Remarkably, an increase in inflammatory cell infiltration of *Gcgr*$^{V369M/V369M}$ mice was not observed until 12 months of age (Fig. 2A and Table S1). Additionally, at 12 months of age, *Gcgr*$^{V369M/V369M}$ mice exhibited liver enlargement compared to WT mice (Fig. S2A). Liver enzymes, such as AST and ALT, indicative of liver damage or disease, showed a mild decrease in the aged *Gcgr*$^{V369M/V369M}$ mice. Importantly, the ratio of AST to ALT remained comparable between the two groups (Fig. 2B–D). Additionally, elevated levels of plasma ALB were noted in aged *Gcgr*$^{V369M/V369M}$ mice (Fig. 2E), suggesting the presence of mild liver inflammation.

3.3. Elevated plasma amino acid levels

Impaired GCGR signaling leads to disrupted amino acid clearance and reduced ureagenesis [20]. To investigate whether this phenotype is present in *Gcgr*$^{V369M/V369M}$ mice, we analyzed plasma amino acid concentrations in 12-month-old mice, a stage when abnormalities in blood glucose and lipid metabolism begin to emerge. A clustering analysis of 42 amino acids showed a substantial increase in most amino acids of *Gcgr*$^{V369M/V369M}$ mice (Fig. 3A); 19 of them increased by 1.4- to 3.3-fold compared to WT mice (Fig. 3B). Glutamine and leucine, which are potent regulators of mTOR, play a role in α-cell hyperplasia [5,21–23]. However, our findings suggest that alanine (Ala), proline (Pro) and the effective GCG secretagogue, arginine (Arg), but not glutamine and leucine, play a role in the pathological alterations of *Gcgr*$^{V369M/V369M}$ mice. This aligns with a previous study indicating that these three amino acids stimulate GCG secretion in female perfused mouse pancreas [24]. Moreover, citrulline (Cit) is converted into Arg in hepatocyte cytoplasm, and Arg is then hydrolyzed into urea and ornithine [25]. Cit increased probably due to the elevated Arg, disturbed amino acid clearance, and decreased ureagenesis [26]. The sole amino acid that declined in the *Gcgr*$^{V369M/V369M}$ group is gamma-aminobutyric acid, by nearly 2-fold, which is a negative regulator of GCG secretion and action. As shown in Fig. 3C, plasma concentrations of glucogenic amino acids (GAA), ketogenic amino acids (KAA) and total α-amino acids (TAA) all increased, while branched-chain amino acids (BCAA), which are known for promoting insulin release, showed no change. These results suggest that hyperaminoacidemia manifested by *Gcgr*$^{V369M/V369M}$ mice involves amino acids mainly related to gluconeogenesis and cell hyperplasia.

The impact of impaired GCG signaling on hepatic amino acid catabolism varies among different diets (Table S2). Ten amino acids (aminoadipic acid, Ala, serine, Cit, Arg, ornithine, threonine, tyrosine, lysine and Pro) increased in *Gcgr*$^{V369M/V369M}$ mice receiving either HFD or RCD. However, only Ser, which plays a role in fat metabolism, increased in SCD, HFD and RCD, indicating a role of dietary factors.

3.4. Pancreatic α-cells hyperplasia

At 12 months of age, the pancreases of *Gcgr*$^{V369M/V369M}$ mice were larger than the WT counterparts (Fig. S2B). However, histological examination revealed a normal morphology (Fig. 4 and Table S3). Besides, *Gcgr*$^{V369M/V369M}$ mice did not progress to PNETs and had a normal lifespan (Fig. S3). GCG staining showed noticeable cell hyperplasia in the pancreatic islets of *Gcgr*$^{V369M/V369M}$ mice (Fig. 5A and B). The α-cell hyperplasia was detectable at the age of 3 months, reaching its peak (occupying the majority of pancreatic islets) at the age of 12 months, and declined by 21 months of age. The GCG area (% of islet area) was 20.5 % at 12-month-old and 14.5 % at 21-month-old, respectively. This was accompanied by elevated levels of GCG throughout the lifespan (Fig. 5C). Nevertheless, α-cell hyperplasia in *Gcgr*$^{V369M/V369M}$ mice was insufficient to induce changes in the levels of GLP-1 and insulin (Fig. S4).

3.5. Upregulation of GADD45G

The hyperplasia of α-cells and the emergence of PNETs in *Gcgr*$^{-/-}$ mice are associated with mTOR signaling [27]. To examine if this mechanism also applies to our model, we conducted a transcriptome analysis of the pancreatic tissues obtained from 12-month-old *Gcgr*$^{V369M/V369M}$ and WT mice. The RNA-seq analysis covering 56,980 genes identified 59 genes that were up-regulated, and 62

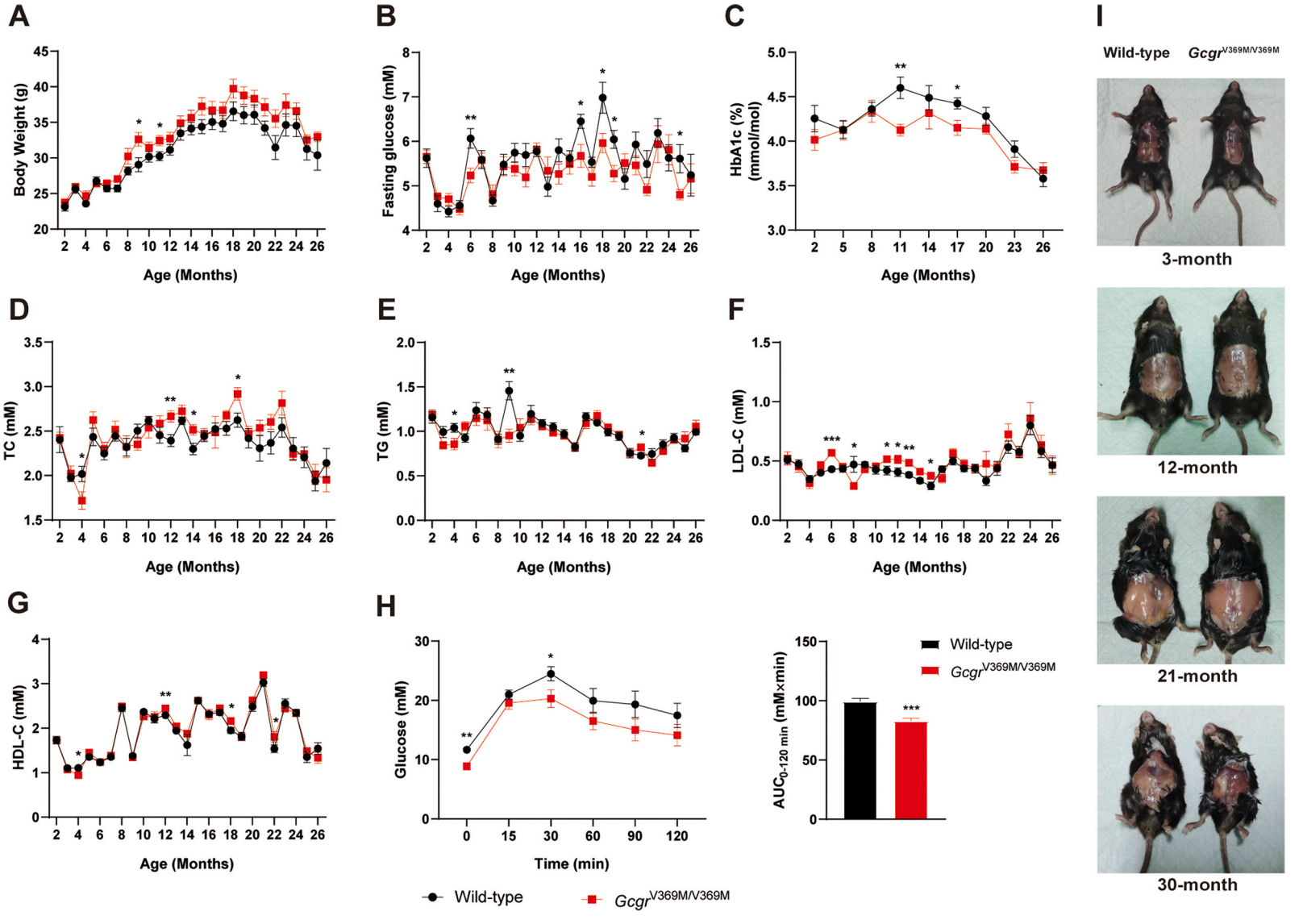

Fig. 1. Gross characteristics of *Gcgr*$^{V369M/V369M}$ mice. Body weight (A), fasting glucose (B), glycated hemoglobin (C) and TC (D), TG (E), LDL-C (F) and HDL-C (G) levels between 2- to 26-month of age in wild-type (WT) and *Gcgr*$^{V369M/V369M}$ mice measured periodically over time (n = 8–12). (H) Glucose tolerance (2 g/kg b.*w*.) in 12-month-old WT and *Gcgr*$^{V369M/V369M}$ mice (n = 9). (I) Anatomical pictures of 3-, 12-, 21- and 30-month-old WT and *Gcgr*$^{V369M/V369M}$ mice. *$P < 0.05$, **$P < 0.01$ and ***$P < 0.001$ using Student's *t*-test compared with the WT mice. HDL-C, high-density lipoprotein cholesterol; LDL-C, low-density lipoprotein cholesterol; TC, total cholesterol; TG, triglycerides.

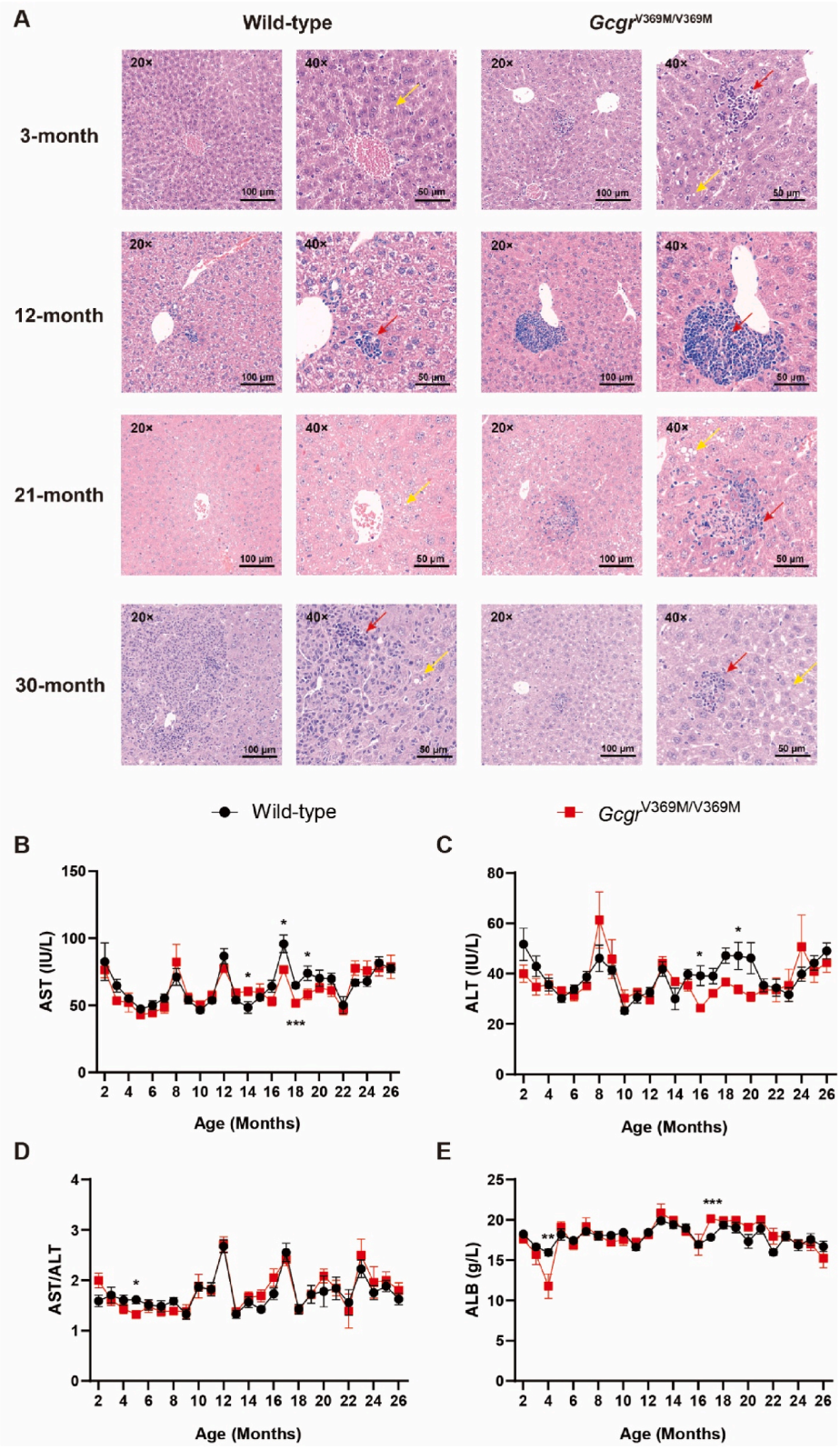

(caption on next page)

Fig. 2. Pathological changes in the liver of *Gcgr*$^{V369M/V369M}$ mice. (A) Microscopy evaluation (H&E staining) was performed on 3-, 12-, 21- and 30-month-old wild-type (WT) and *Gcgr*$^{V369M/V369M}$ mice (n = 5–6). The yellow arrows indicate steatosis, while the red arrows indicate lymphocyte infiltration. Scale bars are shown in the slides. Liver function indicators AST (B), ALT (C), AST/ALT (D) and ALB (E) of WT and *Gcgr*$^{V369M/V369M}$ mice were measured between 2- to 26-month of age (n = 8–12). *$P < 0.05$, **$P < 0.01$ and ***$P < 0.001$ using Student's *t*-test compared with the WT mice. ALB, albumin; ALT, alanine aminotransferase; AST, aspartate aminotransferase.

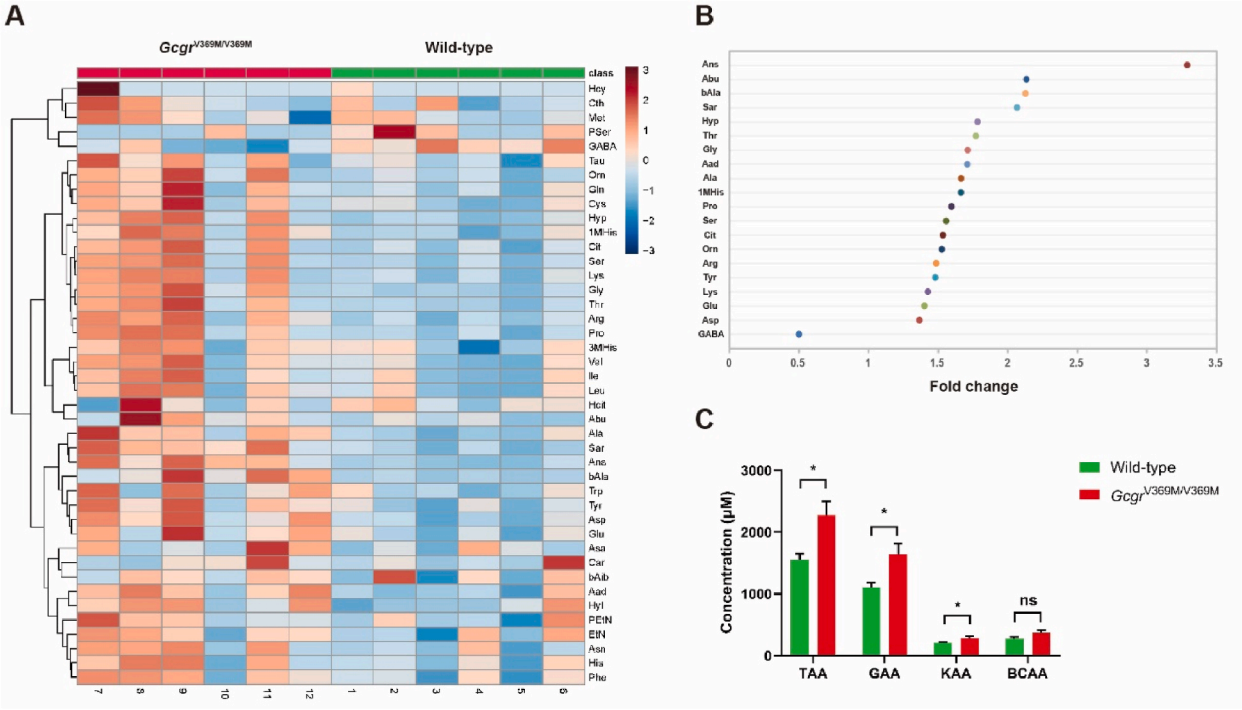

Fig. 3. Amino acid levels in *Gcgr*$^{V369M/V369M}$ mice. (A) Clustering of plasma concentrations of 42 amino acids differentially accumulated in *Gcgr*$^{V369M/V369M}$ (red) and wild-type (WT; green) mice. The scale represents normalized counts derived from variance stabilizing transformation. The gradient color of the graph, ranging from red to blue, indicates high to low concentration levels. The concentrations of plasma amino acid were measured in 12-month-old male mice. (B) Fold change of plasma amino acid levels in *Gcgr*$^{V369M/V369M}$ mice relative to WT mice. (C) Comparison of amino acid levels in *Gcgr*$^{V369M/V369M}$ and WT mice. n = 6. *$P < 0.05$ using Student's *t*-test. BCAA, branched-chain amino acid; GAA, glucogenic amino acid; KAA, ketogenic amino acid; TAA, total α-amino acid.

genes that were down-regulated, respectively (Fig. 6A and Table S4). Compared to WT mice, *Gcgr*$^{V369M/V369M}$ mice showed a significant decrease (P value = 2.72×10^{-2}, log2FC = −2.15) in proline rich 5 like (*PRR5L*), which dissociates from mTORC2 to promote apoptosis [28]. Such a reduction may contribute to α-cell hyperplasia. Meanwhile, the expression of the growth arrest and DNA damage-inducible gamma gene (*GADD45G*), encoding GADD45γ *in vivo*, was most significantly up-regulated (P value = 1.24×10^{-10}, log2FC = 2.29). *GADD45G* has been implicated for anti-tumor property, as it suppressed the growth and epithelial-mesenchymal transition of human breast cancer cells both *in vivo* and *in vitro*, mainly via activation of the MAPK signaling pathway [29]. We assessed *GADD45G* expression in the pancreatic samples that were used for RNA-seq and found an approximately 4-fold increase in *Gcgr*$^{V369M/V369M}$ mice (Fig. 6C), further validating the RNA-seq findings.

Moreover, we observed a 1.9-fold up-regulation (P value = 4.96×10^{-2}, log2FC = 1.13) of angiopoietin-like 4 (*ANGPTL4*), a protein-coding gene known to regulate glucose homeostasis, lipid metabolism, and insulin sensitivity [30]. In contrast to the high expression of *SLC38A* in *Gcgr*$^{-/-}$ mice [31], *SLC6A20A* responsible for Pro transport, was markedly up-regulated (P value = 4.41×10^{-3}, log2FC = 4.18) in *Gcgr*$^{V369M/V369M}$ mice, a feature differs from the phenotype of GCGR knockout. These DEGs were further studied by KEGG enrichment and innovation pathway analyses (Fig. 6B and D), revealing the participation of "amino acid metabolism", "bile secretion", "cell growth and death", "IL-17 signaling pathway", "PPAR signaling pathway" and "sugar biosynthesis". Among these pathways, the most significantly enriched is mucin type *O*-glycan biosynthesis (adjusted P value = 0.23, rich factor = 0.0625), followed by other type *O*-glycan biosynthesis (adjusted P value = 0.27, rich factor = 0.0465). Glycosylation of mucin type *O*-glycans can occur on amino acids with functional hydroxyl groups, such as Ser and Thr [32], all of which displayed increased levels in *Gcgr*$^{V369M/V369M}$ mice.

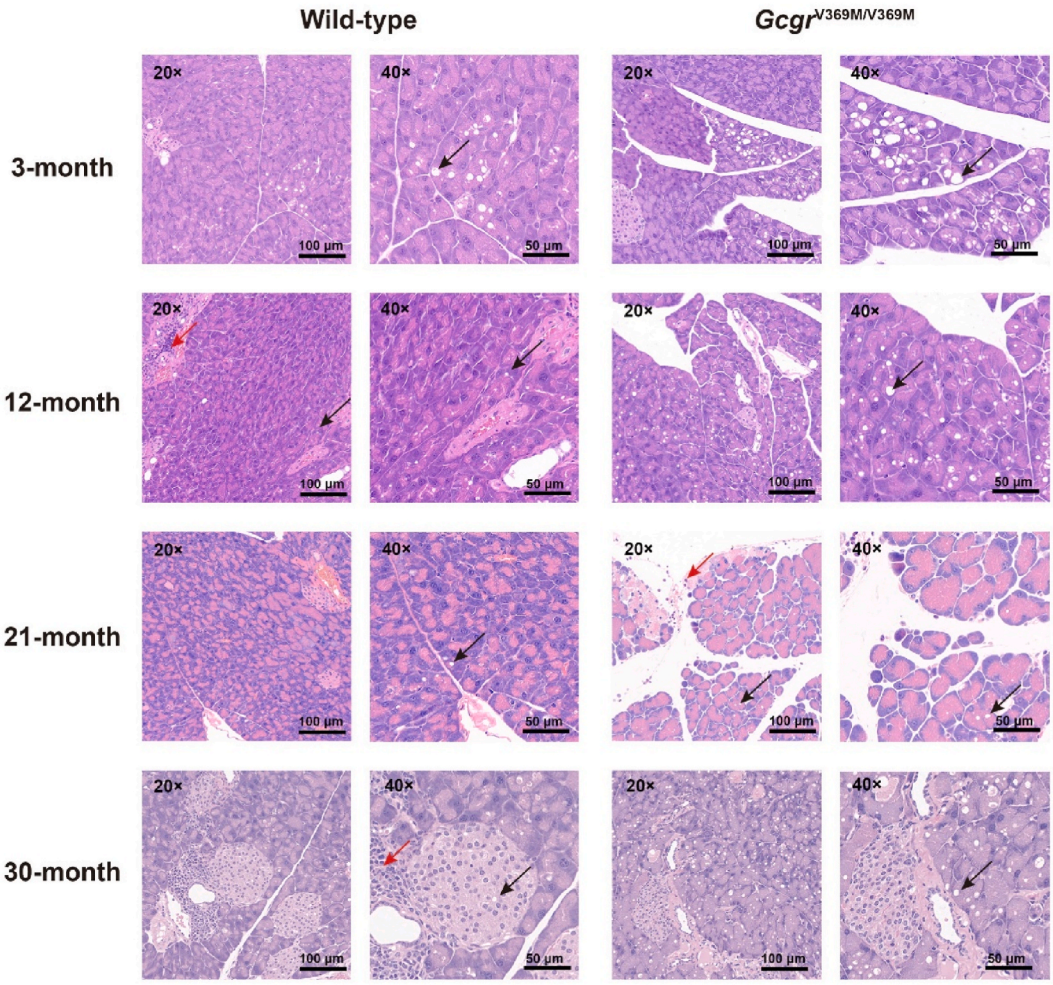

Fig. 4. Pathological changes in the pancreas of *Gcgr*$^{V369M/V369M}$ mice. (A) Microscopy evaluation (H&E staining) of the 3-, 12-, 21- and 30-month-old wild-type (WT) and *Gcgr*$^{V369M/V369M}$ mice (n = 5–6). The black arrows represent the autophagic vacuoles of acinar cells, while the red arrows indicate lymphocyte infiltration. Scale bars are shown in the slides.

4. Discussion

In the present study, we not only confirmed our prior observations of reduced blood glucose, elevated GCG and amino acid levels, but also demonstrated α-cell hyperplasia in *Gcgr*$^{V369M/V369M}$ mice at all stages, similar to that seen in *Gcgr*$^{-/-}$ mice. In younger mice (3-month-old), α-cell hyperplasia predominates without clear enlargement of the pancreas. By 12 months of age, pancreas enlargement becomes apparent, but it diminishes by the time the mice reach 21 months. The sustained α-cell hyperplasia observed throughout the lifespan of *Gcgr*$^{V369M/V369M}$ mice underscores the chronic nature of Mahvash disease and highlights the importance of long-term monitoring to understand disease progression. It is known that disrupted GCG signaling leads to PNETs in mice with *Gcgr* deletion and in humans with inactivating mutations in GCGR [33]. Despite prolonged α-cell hyperplasia and elevated GCG levels, the absence of PNETs in *Gcgr*$^{V369M/V369M}$ mice suggests that additional factors or genetic alterations may be required for tumor formation. The observed outcomes suggest a "dose effect" of the GCGR mutation on the mice. Complete GCGR deletion results in the most severe phenotype, including the development of PNETs and very high glucagon levels. In contrast, a partially inactivating mutation like V369M only has subtle effects.

It appears that incomplete inhibition of GCG signaling may induce a compensatory increase in α-cell mass and elevated GCG secretion, involving circulating amino acids such as Ala, Pro, and Arg. This feedback loop supports the presence of a liver–α-cell axis. A recent case report found that hepatocyte-specific overexpression of WT GCGR could be a potential therapeutic strategy for Mahvash disease. A woman with Mahvash disease who had a liver transplant demonstrated normalized serum glucagon and ammonia levels, as well as a reversal of pancreatic hypertrophy [34].

Previous studies have shown that primary hepatocytes isolated from 20- to 25-week-old female *Gcgr*$^{V369M/V369M}$ mice exhibited reduced ^{125}I-glucagon binding and decreased glucagon potency, leading to lower fasting blood glucose levels [9]. In this paper, young

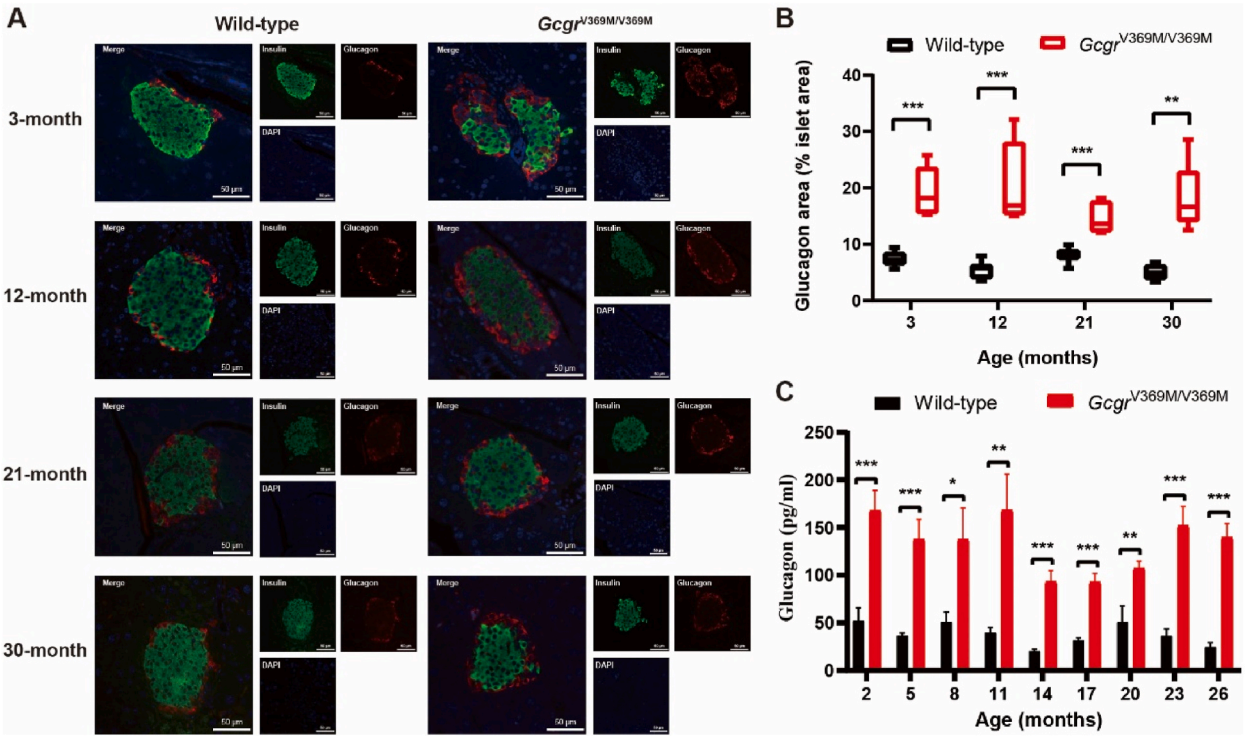

Fig. 5. Hyperplasia of α-cells in *Gcgr*$^{V369M/V369M}$ mice. Immunofluorescence staining of the pancreas (A) and glucagon area (% of the islet area) (B) in 3-, 12-, 21- and 30-month-old wild-type (WT) and *Gcgr*$^{V369M/V369M}$ mice. Insulin (green) and glucagon (red) were visualized by immunofluorescence staining while the nuclei (blue) by DAPI. Bars indicate 50 μm. n = 5–6. (C) Glucagon concentration in plasma of WT and *Gcgr*$^{V369M/V369M}$ mice between 2- to 26-month of age (n = 6–8). *$P < 0.05$, **$P < 0.01$ and ***$P < 0.001$ using Student's *t*-test compared with the WT mice.

Gcgr$^{V369M/V369M}$ mice displayed significantly reduced fasting glucose and elevated cholesterol and low-density lipoprotein-cholesterol levels. However, as the mutant mice aged, their physiological indicators became similar to those of WT mice. In aging mutant mice, adaptive glucose and lipid metabolism occurred to compensate for GCGR abnormality. Meanwhile, aging WT mice may experience liver dysfunction, leading to decreased insulin sensitivity and a decline in GCGR function. This results in ineffective glycogen breakdown, abnormal gluconeogenesis, and disrupted lipid metabolism. Interestingly, such an adaptation in aging mutant mice also decelerates α-cell hyperplasia, likely due to prolonged suppression of GCGR signaling in *Gcgr*$^{V369M/V369M}$ mice. These findings are consistent with our RNA-seq data. *GADD45G*, known for initiating embryonic stem cell differentiation and inhibiting breast cancer cell carcinogenesis [29], was the most significantly upregulated gene, suggesting a mechanism by which α-cell hyperplasia and tumor formation are contained. The potential role of *GADD45G* in α-cell hyperplasia throughout life is worth further investigation. Likewise, increased expression of *ANGPTL4* and *SLC6A20A* implies the involvement of additional pathways. In addition, the results of the KEGG pathway analysis align with the observed changes in amino acid metabolism in *Gcgr*$^{V369M/V369M}$ mice, indicating the upregulation of amino acids (Ser and Thr) that can undergo glycosylation of mucin *O*-glycans. Overall, our study offers an accessible mouse model of Mahvash disease, characterized by initial α-cell dysplasia followed by metabolic adaptation including reduction of GCG and restoration of α-cell mass.

5. Conclusion

In conclusion, our study demonstrated that *Gcgr*$^{V369M/V369M}$ mice, the mouse model of mild Mahvash disease, exhibited reduction in fasting blood glucose levels, elevated cholesterol and LDL-C levels, hyperaminoacidemia, and α-cell hyperplasia with increased GCG levels at a young age. However, metabolic disparities between WT mice and *Gcgr*$^{V369M/V369M}$ mice waned with age.

Data availability statement

The source data of this study will be available from the corresponding author on reasonable request.

Ethics declarations

This study was reviewed and approved by the Animal Ethics Committee, with the IACUC approval number: 2022-02-YDH-01.

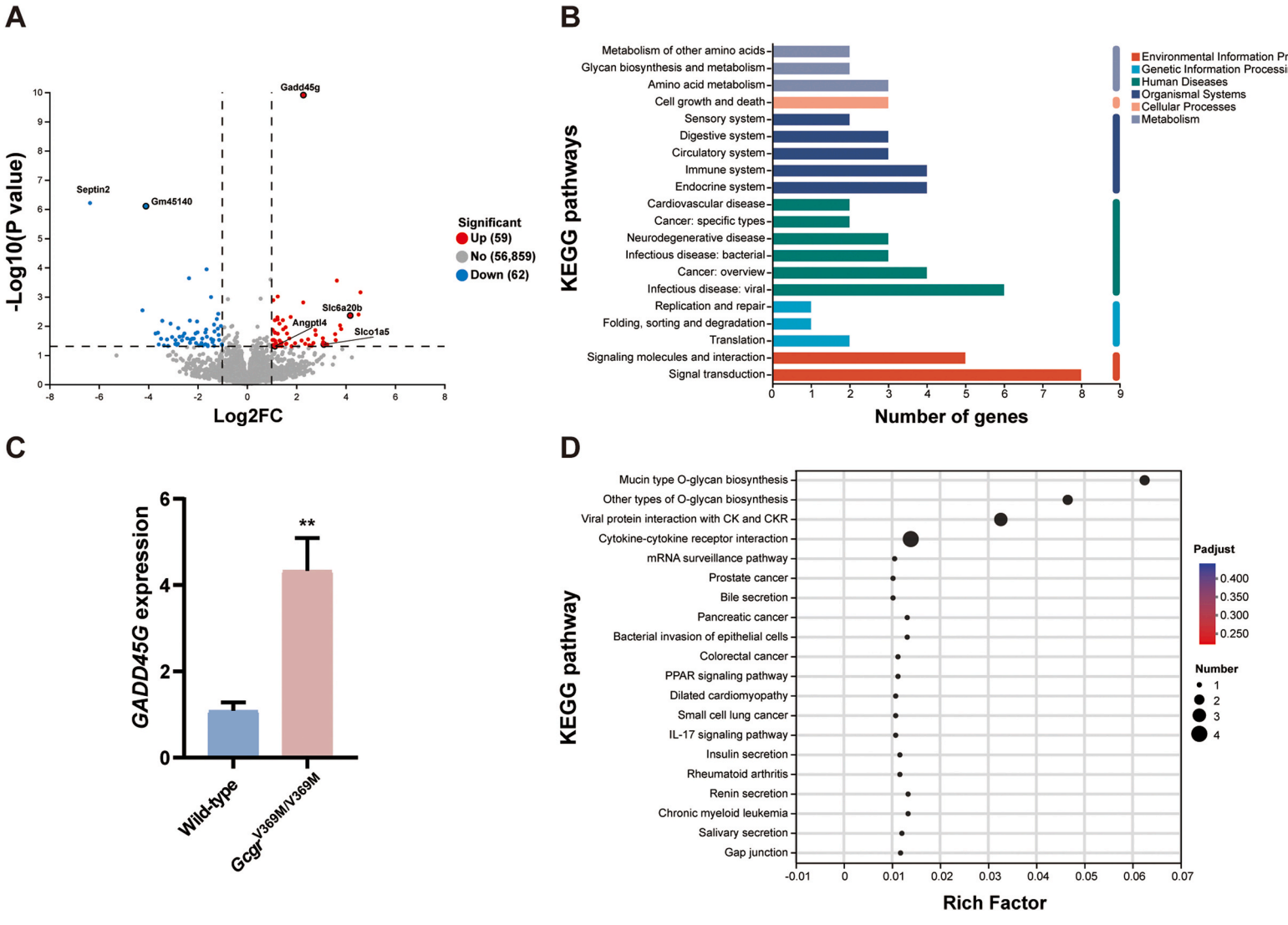

Fig. 6. RNA-seq analysis of the pancreas in 12-month-old mice. (A) Volcano plot of DEGs (FDR<0.05) in wild-type (WT) and *Gcgr*$^{V369M/V369M}$ mice. The horizontal axis represents the log2 fold change between WT and *Gcgr*$^{V369M/V369M}$ genes, while the vertical axis represents the negative log10 of the P value from the Fisher's exact test. Each point on the graph corresponds to a single gene. (B) Pathway over-representation analysis utilizing the KEGG database was conducted on genes from each of the clusters. (C) Real-time PCR detection of *GADD45G* expression in the pancreas of WT and *Gcgr*$^{V369M/V369M}$ mice. Data are presented as means ± S.E.M. and were conducted in quadruplicate. (D) Ingenuity Pathway Analysis of the RNA-seq data was employed to predict signaling pathway activity. Statistical significance was determined by Student's *t*-test, with $^{*}P < 0.05$ and $^{**}P < 0.01$ compared with the WT mice (n = 4–5).

Funding statement

This work was partially supported by the National Natural Science Foundation of China 82273961(M.-W.W.), 81872915 (M.-W.W.), 82073904 (M.-W.W.), 82273985 (D.H.Y.), 81973373 (D.H.Y.) and 82121005 (D.H.Y.); National Science & Technology Major Project of China—Key New Drug Creation and Manufacturing Program 2018ZX09735–001 (M.-W.W.) and 2018ZX09711002–002–005 (D.H.Y.); STI2030-Major Project 2021ZD0203400 (Q.T.Z.); the National Key Basic Research Program of China 2023YFA1800804 (D.H.Y.); Hainan Provincial Major Science and Technology Project ZDKJ2021028 (Q.T.Z. and D.H.Y.); Program of Shanghai Academic/Technology Research Leader 23XD1400900 (D.H.Y.) and Shanghai Municipality Science and Technology Development Fund 21JC1401600 (D.H.Y.).

CRediT authorship contribution statement

Yingna Xu: Conceptualization, Formal analysis, Investigation, Methodology, Software, Writing – original draft. **Qiaofeng Liu:** Formal analysis, Investigation, Methodology, Software. **Chuan-Wei Chen:** Methodology. **Qiuying Wang:** Methodology. **Tianyuan Du:** Methodology. **Run Yu:** Conceptualization, Writing – review & editing. **Qingtong Zhou:** Funding acquisition, Writing – review & editing. **Dehua Yang:** Funding acquisition, Supervision, Validation, Writing – review & editing. **Ming-Wei Wang:** Conceptualization, Funding acquisition, Project administration, Supervision, Writing – review & editing.

Declaration of competing interest

The authors declare no competing interests related to the present study.

Acknowledgements

We are grateful to Minbo Hou for technical assistance.

Appendix A. Supplementary data

Supplementary data to this article can be found online at https://doi.org/10.1016/j.heliyon.2024.e35362.

List of abbreviations

Ala	alanine
ALB	albumin
ALT	alanine aminotransferase
ANGPTL4	angiopoietin-like 4
Arg	arginine
AST	aspartate aminotransferase
BCAA	branched-chain amino acids
Ca^{2+}	calcium ion
cAMP	cyclic adenosine monophosphate
DEGs	differentially expressed genes
ECL3	extracellular loop 3
FDR	false discovery rate
GAA	glucogenic amino acids
GADD45G	growth arrest and DNA damage-inducible gamma gene
GCG	glucagon
GCGR	glucagon receptor
GCGR	glucagon receptor gene
GLP-1	glucagon-like peptide-1
GO	Gene Ontology
HbA_{1c}	Hemoglobin A1c
H&E	hematoxylin and eosin
HDL-C	high-density lipoprotein-cholesterol
HFD	high-fat diet
|log2FC|	absolute log2 fold change
KEGG	Kyoto Encyclopedia of Genes and Genomes
KAA	ketogenic amino acids
LDL	low-density lipoprotein
LDL-C	low-density lipoprotein-cholesterol
mTOR	mammalian target of rapamycin

PFA	paraformaldehyde
PNETs	pancreatic neuroendocrine tumors
Pro	proline
qRT-PCR	quantitative reverse transcription polymerase chain reaction
RCD	regular chow diet
RNA-seq	RNA-sequencing
SCD	standard chow diet
S.E.M	standard error of the mean
SPF	specific-pathogen–free
TAA	total α-amino acids
TC	total cholesterol
TG	triglycerides
WT	wild-type

References

[1] R.H. Unger, A.M. Eisentraut, C.M. Mc, L.L. Madison, Measurements of endogenous glucagon in plasma and the influence of blood glucose concentration upon its secretion, J. Clin. Invest. 41 (4) (1962) 682–689.
[2] R.P. Eaton, Hypolipemic action of glucagon in experimental endogenous lipemia in the rat, J. Lipid Res. 14 (3) (1973) 312–318.
[3] E.D. Dean, R.H. Unger, W.L. Holland, Glucagon antagonism in islet cell proliferation, Proc Natl Acad Sci U S A 114 (12) (2017) 3006–3008.
[4] R.W. Gelling, X.Q. Du, D.S. Dichmann, J. Romer, H. Huang, L. Cui, S. Obici, B. Tang, J.J. Holst, C. Fledelius, P.B. Johansen, L. Rossetti, L.A. Jelicks, P. Serup, E. Nishimura, M.J. Charron, Lower blood glucose, hyperglucagonemia, and pancreatic alpha cell hyperplasia in glucagon receptor knockout mice, Proc Natl Acad Sci U S A 100 (3) (2003) 1438–1443.
[5] M.J. Solloway, A. Madjidi, C. Gu, J. Eastham-Anderson, H.J. Clarke, N. Kljavin, J. Zavala-Solorio, L. Kates, B. Friedman, M. Brauer, J. Wang, O. Fiehn, G. Kolumam, H. Stern, J.B. Lowe, A.S. Peterson, B.B. Allan, Glucagon couples hepatic amino acid catabolism to mTOR-dependent regulation of alpha-cell mass, Cell Rep. 12 (3) (2015) 495–510.
[6] R. Yu, D. Dhall, N.N. Nissen, C. Zhou, S.G. Ren, Pancreatic neuroendocrine tumors in glucagon receptor-deficient mice, PLoS One 6 (8) (2011) e23397.
[7] R. Yu, Mahvash disease: 10 years after discovery, Pancreas 47 (5) (2018) 511–515.
[8] W.J.C. van der Velden, P. Lindquist, J.S. Madsen, R.H.M.J. Stassen, N.J. Wewer Albrechtsen, J.J. Holst, A.S. Hauser, M.M. Rosenkilde, Molecular and in vivo phenotyping of missense variants of the human glucagon receptor, J. Biol. Chem. 298 (2) (2022) 101413.
[9] G. Lin, Q. Liu, A. Dai, X. Cai, Q. Zhou, X. Wang, Y. Chen, C. Ye, J. Li, D. Yang, M.W. Wang, Characterization of a naturally occurring mutation V368M in the human glucagon receptor and its association with metabolic disorders, Biochem. J. 477 (13) (2020) 2581–2594.
[10] Q. Liu, G. Lin, Y. Chen, W. Feng, Y. Xu, J. Lyu, D. Yang, M.W. Wang, Deleterious mutation V369M in the mouse GCGR gene causes abnormal plasma amino acid levels indicative of a possible liver-alpha-cell axis, Biosci. Rep. 41 (6) (2021) BSR20210758.
[11] A.H. Fischer, K.A. Jacobson, J. Rose, R. Zeller, Hematoxylin and eosin staining of tissue and cell sections, CSH Protoc 2008 (2008) pdb prot4986.
[12] S. Chen, Y. Zhou, Y. Chen, J. Gu, fastp: an ultra-fast all-in-one FASTQ preprocessor, Bioinformatics 34 (17) (2018) i884–i890.
[13] D. Kim, B. Langmead, S.L. Salzberg, HISAT: a fast spliced aligner with low memory requirements, Nat. Methods 12 (4) (2015) 357–360.
[14] M. Pertea, G.M. Pertea, C.M. Antonescu, T.C. Chang, J.T. Mendell, S.L. Salzberg, StringTie enables improved reconstruction of a transcriptome from RNA-seq reads, Nat. Biotechnol. 33 (3) (2015) 290–295.
[15] B. Li, C.N. Dewey, RSEM: accurate transcript quantification from RNA-Seq data with or without a reference genome, BMC Bioinf. 12 (2011) 323.
[16] M.I. Love, W. Huber, S. Anders, Moderated estimation of fold change and dispersion for RNA-seq data with DESeq2, Genome Biol. 15 (12) (2014) 550.
[17] L. Wang, Z. Feng, X. Wang, X. Wang, X. Zhang, DEGseq: an R package for identifying differentially expressed genes from RNA-seq data, Bioinformatics 26 (1) (2010) 136–138.
[18] C. Xie, X. Mao, J. Huang, Y. Ding, J. Wu, S. Dong, L. Kong, G. Gao, C.Y. Li, L. Wei, Kobas 2.0: a web server for annotation and identification of enriched pathways and diseases, Nucleic Acids Res. 39 (2011) W316–W322.
[19] H. Li, L. Zhao, R. Singh, J.N. Ham, D.O. Fadoju, L.J.H. Bean, Y. Zhang, Y. Xu, H.E. Xu, M.J. Gambello, The first pediatric case of glucagon receptor defect due to biallelic mutations in GCGR is identified by newborn screening of elevated arginine, Mol Genet Metab Rep 17 (2018) 46–52.
[20] K.D. Galsgaard, M. Winther-Sørensen, J. Pedersen, S.A.S. Kjeldsen, M.M. Rosenkilde, N.J. Wewer Albrechtsen, J.J. Holst, Glucose and amino acid metabolism in mice depend mutually on glucagon and insulin receptor signaling, Am. J. Physiol. Endocrinol. Metab. 316 (4) (2019) E660–E673.
[21] E.D. Dean, M. Li, N. Prasad, S.N. Wisniewski, A. Von Deylen, J. Spaeth, L. Maddison, A. Botros, L.R. Sedgeman, N. Bozadjieva, O. Ilkayeva, A. Coldren, G. Poffenberger, A. Shostak, M.C. Semich, K.I. Aamodt, N. Phillips, H. Yan, E. Bernal-Mizrachi, J.D. Corbin, K.C. Vickers, S.E. Levy, C. Dai, C. Newgard, W. Gu, R. Stein, W. Chen, A.C. Powers, Interrupted glucagon signaling reveals hepatic alpha cell axis and role for L-glutamine in alpha cell proliferation, Cell Metab 25 (6) (2017) 1362–13673 e5.
[22] J. Kim, H. Okamoto, Z. Huang, G. Anguiano, S. Chen, Q. Liu, K. Cavino, Y. Xin, E. Na, R. Hamid, J. Lee, B. Zambrowicz, R. Unger, A.J. Murphy, Y. Xu, G. D. Yancopoulos, W.H. Li, J. Gromada, Amino acid transporter Slc38a5 controls glucagon receptor inhibition-induced pancreatic alpha cell hyperplasia in mice, Cell Metab 25 (6) (2017) 1348–13461 e8.
[23] S.M. Son, S.J. Park, H. Lee, F. Siddiqi, J.E. Lee, F.M. Menzies, D.C. Rubinsztein, Leucine signals to mTORC1 via its metabolite acetyl-coenzyme A, Cell Metab 29 (1) (2019) 192–201 e7.
[24] K.D. Galsgaard, S.L. Jepsen, S.A.S. Kjeldsen, J. Pedersen, N.J. Wewer Albrechtsen, J.J. Holst, Alanine, arginine, cysteine, and proline, but not glutamine, are substrates for, and acute mediators of, the liver-alpha-cell axis in female mice, Am. J. Physiol. Endocrinol. Metab. 318 (6) (2020) E920–E929.
[25] T.J. Fujimi, Y. Mezaki, T. Masaki, A. Tajima, M. Nakamura, A. Yoshikawa, N. Murai, M. Aizawa, S. Kojima, Y. Matsumoto, H. Aizaki, T. Matsuura, Investigation of the effects of urea cycle amino acids on the expression of ALB and CEBPB in the human hepatocellular carcinoma cell line FLC-4, Hum. Cell 33 (3) (2020) 590–598.
[26] M. Winther-Sørensen, K.D. Galsgaard, A. Santos, S.A.J. Trammell, K. Sulek, R.E. Kuhre, J. Pedersen, D.B. Andersen, A.S. Hassing, M. Dall, J.T. Treebak, M. P. Gillum, S.S. Torekov, J.A. Windeløv, J.E. Hunt, S.A.S. Kjeldsen, S.L. Jepsen, C.G. Vasilopoulou, F.K. Knop, C. Ørskov, M.P. Werge, H.C. Bisgaard, P.L. Eriksen, H. Vilstrup, L.L. Gluud, J.J. Holst, N.J. Wewer Albrechtsen, Glucagon acutely regulates hepatic amino acid catabolism and the effect may be disturbed by steatosis, Mol Metab 42 (2020) 101080.
[27] Y. Jiao, C. Shi, B.H. Edil, R.F. de Wilde, D.S. Klimstra, A. Maitra, R.D. Schulick, L.H. Tang, C.L. Wolfgang, M.A. Choti, V.E. Velculescu, L.A. Diaz Jr., B. Vogelstein, K.W. Kinzler, R.H. Hruban, N. Papadopoulos, DAXX/ATRX, MEN1, and mTOR pathway genes are frequently altered in pancreatic neuroendocrine tumors, Science 331 (6021) (2011) 1199–1203.
[28] K. Thedieck, P. Polak, M.L. Kim, K.D. Molle, A. Cohen, P. Jenö, C. Arrieumerlou, M.N. Hall, PRAS40 and PRR5-like protein are new mTOR interactors that regulate apoptosis, PLoS One 2 (11) (2007) e1217.

[29] X. Zhang, Y. Li, J. Ji, X. Wang, M. Zhang, X. Li, Y. Zhang, Z. Zhu, S.D. Ye, X. Wang, Gadd45g initiates embryonic stem cell differentiation and inhibits breast cell carcinogenesis, Cell Death Discov 7 (1) (2021) 271.
[30] B. Aryal, N.L. Price, Y. Suarez, C. Fernandez-Hernando, ANGPTL4 in metabolic and cardiovascular disease, Trends Mol. Med. 25 (8) (2019) 723–734.
[31] D.K. Smith, L. Kates, S. Durinck, N. Patel, E.W. Stawiski, N. Kljavin, O. Foreman, B. Sipos, M.J. Solloway, B.B. Allan, A.S. Peterson, Elevated serum amino acids induce a subpopulation of alpha cells to initiate pancreatic neuroendocrine tumor formation, Cell Rep Med 1 (5) (2020) 100058.
[32] C. Reily, T.J. Stewart, M.B. Renfrow, J. Novak, Glycosylation in health and disease, Nat. Rev. Nephrol. 15 (6) (2019) 346–366.
[33] C. Zhou, D. Dhall, N.N. Nissen, C.R. Chen, R. Yu, Homozygous P86S mutation of the human glucagon receptor is associated with hyperglucagonemia, alpha cell hyperplasia, and islet cell tumor, Pancreas 38 (8) (2009) 941–946.
[34] J. Robbins, D. Halegoua-DeMarzio, A. Basu Mallick, N. Vijayvergia, R. Ganetzky, H. Lavu, V.N. Giri, J. Miller, W. Maley, A.P. Shah, M. DiMeglio, M. Ambelil, R. Yu, T. Sato, D.S. Lefler, Liver transplantation in a woman with mahvash disease, N. Engl. J. Med. 389 (21) (2023) 1972–1978.